CHARACTERIZATION OF ELECTROSTATIC GAP-CLOSING ACTUATOR ARRAYS IN AQUEOUS CONDITIONS

Ryan M. Shih, Daniel S. Contreras, Travis L. Massey, Joseph T. Greenspun, and Kristofer S. J. Pister
Berkeley Sensor & Actuator Center
Electrical Engineering and Computer Sciences, UC Berkeley, USA

ABSTRACT

We demonstrate high-force-density rapid actuation of electrostatic gap-closing actuator (GCA) arrays operating in an aqueous environment. These devices are designed to generate up to 4.6 mN at 6 V drive signal amplitudes and have measured pull-in times as fast as 121 µs with no electrolysis. We present a new model for the dynamics of aqueous GCA operation which includes the inertia of the squeezed fluid and proximity of the substrate to the device layer. The actuators operate in deionized water, and preliminary tests demonstrate actuation in ionic solutions (10 mM) and partial operation of submerged inchworm motors based on GCA arrays.

INTRODUCTION

Aqueous MEMS Applications

Most MEMS applications involve devices operating in air or vacuum. However, design for aqueous environments opens new avenues of research in fields like biology, microfluidics, and medicine. Electrostatic devices in particular benefit from the relative permittivity factor, often much greater than 1 for liquids, producing greater actuation forces with smaller drive voltages. To realize this benefit, however, device design must address several challenges not encountered in air or vacuum.

Challenges in Aqueous Operation

According to Sameoto et. al [1], there are three significant problems that must be overcome for electrostatic MEMS operation in liquid. These are surface tension, electrolysis, and electrical conductivity. Surface tension of the liquid can cause stiction if devices are dried, but of greater concern is the trapping of gas bubbles that can interfere with device behavior. These problems are best addressed by submerging devices slowly to prevent bubble trapping and storing them in sealed containers to minimize evaporation losses. The second challenge is electrolysis, which can also create gas bubbles and may lead to other chemical reactions that alter the electrodes or liquid medium. However, Sounart et. al [2] demonstrated that electrolysis can be prevented by use of a high-frequency alternating-current (AC) drive signal instead of a direct-current (DC) drive signal. The third challenge is related to the medium itself. Liquids with high electrical conductivity will dissipate power, reducing the efficiency of the electrostatic actuator. As some applications will dictate the medium, this challenge may be unavoidable. If the medium can be chosen however, ionic content should be minimized. Successful operation of an electrostatic MEMS device in liquid can thus be best achieved through 1) careful design and handling, 2) a high-frequency AC drive signal, and 3) selection of media with low ionic content if possible.

Electrostatic MEMS in Aqueous Environments

For our projected application space, namely the design of microrobots for aqueous environments, actuators should exhibit significant and controllable displacement (several hundred microns), high output forces (greater than 1 mN), and fast operation times (less than 1 ms). Of the many MEMS devices that are driven using electrostatics, very few operate in aqueous environments, and fewer to date come close to meeting these characteristics. Devices have been tested successfully in water and other solutions [2-6] but have limited displacement (less than 50 µm), low forces (less than 50 µN), and little characterization of operation times. The state of the art in electrostatic MEMS for aqueous environments thus has substantial room for improvement. A potential solution is the inchworm motor based on gap-closing actuator (GCA) arrays introduced by Penskiy and Bergbreiter [7]. These achieve high efficiency, displacements, and forces with fast actuation times in air [8]. We seek to develop similar motors for operation in aqueous environments, but to do so first requires characterization of GCA arrays in aqueous conditions.

THEORY

Gap-Closing Actuator Dynamics

In this work, we characterize GCA arrays in deionized water. GCA arrays are devices that rely on attractive electrostatic forces to move one set of plates (colloquially termed "fingers") closer to an interdigitated set of adjacent plates. This is achieved by grounding one electrode, such as the anchored fingers, and driving the other electrode (moveable fingers in this case) with a voltage signal. With appropriate spacing between grounded and voltage-driven plates, a non-linear electrostatic force causes the moveable plates to close the gaps between fingers. A free body diagram of a GCA unit cell is shown in Figure 1.

The dynamics of a GCA are determined by

$$F = m_{eff}\ddot{x} + b_{T,adj}(x)\dot{x} + kx \qquad (1)$$

where F is the electrostatic force, m_{eff} is the effective mass of the shuttle and moveable fingers (with inertial effects of the fluid), $b_{T,adj}(x)$ is the adjusted displacement-dependent squeeze film damping coefficient, k is the spring constant of the support springs, and x is displacement. A critical parameter for operation is pull-in time, defined as the time to close completely after the drive signal reaches the GCA. This is determined by solving Equation (1) with initial conditions $x(0) = 0$ and $\dot{x}(0) = 0$.

The electrostatic force for a GCA is calculated from changes in capacitance in device fingers and is given by

$$F = \frac{1}{2}N\epsilon_0\epsilon_r LTV^2\left(\frac{1}{(g_0 - x)^2} - \frac{1}{(g_b + x)^2}\right) \qquad (2)$$

where N is the number of GCA unit cells, ϵ_0 is the

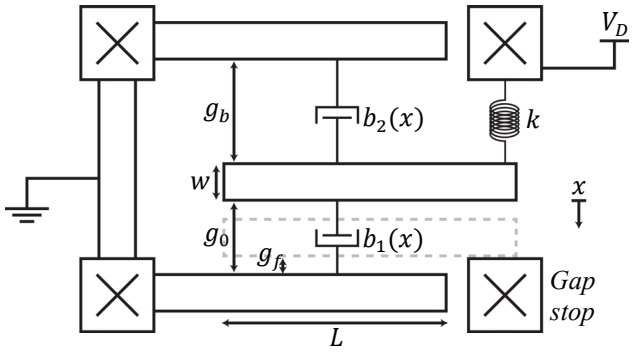

Figure 1: Free body diagram of GCA unit cell (bottom two fingers) and an anchored finger in the adjacent unit cell.

permittivity of free space, ϵ_r is the relative permittivity, L is the overlap length, T is the thickness of the fingers (into the page), V is the zero to peak amplitude of the AC square wave V_D, g_0 is the initial gap between unit cell fingers, g_b is the gap between unit cells, and x is the displacement.

In air, the mass used in Equation (1) would be associated with the shuttle and moveable fingers. In water, however, the inertial effects of fluid movement result in a greater effective mass. This effect is observed as a result of the law of continuity in fluid mechanics. For a plate moving in a fluid toward an identical fixed plate, the flow of fluid squeezed out of the gap is given by

$$A_f \dot{x}_f = A_p \dot{x}_p \tag{3}$$

where A_f is the effective area over which fluid moves, $\dot{x}_f$ is the velocity of fluid through that area, A_p is the area of the plate, and $\dot{x}_p$ is the velocity of the plate. If the moving and fixed plates are the top and bottom faces of a rectangular prism, A_f is the sum of the remaining four face areas. As the gap between fingers shrinks in a GCA unit cell, the mass of the fluid in the gap and velocity of fluid at the plate edges based on Equation (3) are given by

$$m_{f1} = \rho_f LT(g_0 - x) \tag{4}$$

$$\dot{x}_{f1} = \frac{LT\dot{x}_p}{2(g_0 - x)(L + T)} \tag{5}$$

where ρ_f is the density of the fluid and $\dot{x}_p = \dot{x}$. A similar analysis can be done for the growing gap between adjacent unit cells (terms denoted with a subscript of 2). Incorporating the inertial effects of fluid in both gaps, the inertial term of the forcing equation is then given by

$$m_{eff}\ddot{x} = \frac{d}{dt}\left(m\dot{x} + N\left(m_{f1}\frac{\dot{x}_{f1}}{2} + m_{f2}\frac{\dot{x}_{f2}}{2}\right)\right) \tag{6}$$

where m is the nominal mass of the device shuttle and moveable fingers and $\dot{x}_f$ terms are halved to give the average velocity of fluid in the gaps. Plugging Equations (4) and (5) into (6) results in an effective mass that includes the inertial effects of fluid given by

$$m_{eff} = m + \frac{N\rho_f L^2 T^2}{2(L + T)} \tag{7}$$

The squeeze film damping coefficient is calculated based on the Reynolds equation for an incompressible fluid between two rectangular plates. Using GCA dimensions and adding the squeeze film effects of the unit cell, $b_1(x)$, and between adjacent unit cells, $b_2(x)$, Bao and Yang's [9] reported total coefficient is given by

$$b_T(x) = N\mu_f LT^3\beta(\eta)\left(\frac{1}{(g_0 - x)^3} + \frac{1}{(g_b + x)^3}\right) \tag{8}$$

where μ_f is the coefficient of viscosity of the fluid and $\beta(\eta)$ is a correction factor based on the plate aspect ratio.

Li et. al [10] expand upon this finding, accounting for the proximity of substrate beneath the plates. Using GCA dimensions, their adjusted coefficient is given by

$$b_{T,adj}(x) = b_T(x) \cdot \frac{4g_0^3 w + 2g_s^3 T}{g_0^3 w + 2g_s^3 T} \tag{9}$$

where w is the finger width and g_s is the gap between the bottom of the fingers and the underlying substrate. Li et. al use a plate dimension T^* but we do not consider this adjustment as it assumes the squeeze film to be a gas and plate dimensions to be comparable to the separating gap.

The spring constant of the shuttle's support beams is calculated based on Eulerian beam theory and is given by

$$k = \frac{2ETw_s^3}{l_s^3} \tag{10}$$

where E is the Young's Modulus of silicon, w_s is the width of the springs, and l_s is the length of the springs. Substituting (2), (7), (9), and (10) into (1) produces our new model for GCA dynamics in an aqueous environment.

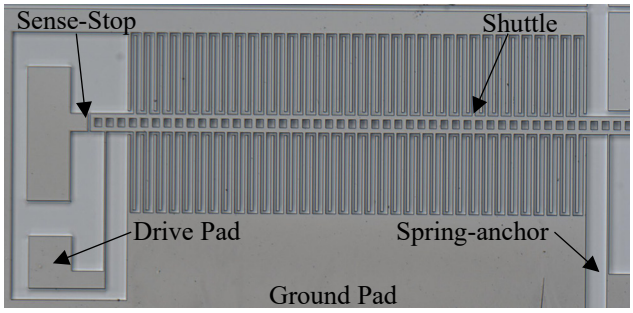

Figure 2: A fabricated GCA. Driving the shuttle with V_D induces pull-in which is measured at the sense-stop. Finger array is 335 μm by 790 μm.

DESIGN AND FABRICATION

GCA Design

A GCA based on those examined by Contreras et. al [8] is shown in Figure 2. The spring-anchor and shuttle are driven with an AC square wave centered about 0 V. Anchored fingers are grounded. The sense-stop serves as both the sense pad for pull-in measurements as well as the gap stop for the shuttle to prevent fingers from shorting.

Fabrication

The GCA devices are fabricated using the silicon-on-insulator (SOI) process described in [8]. They have a 40

µm thick device layer with 2 µm underlying oxide. Metal selection was critical because strong adhesion is required for aqueous conditions. Cr/Ru was selected over the Au/Pd layer utilized in [8] because of its strong adhesion to silicon in submerged devices and the added benefit that its oxide is conductive [11].

METHODS AND RESULTS

GCA finger dimensions were 4 µm in width (w) with variable overlap lengths (L) ranging from 10 µm to 130 µm in 15 µm increments. The gaps in unit cells (g_0) and between unit cells (g_b) were 5.83 µm and 8.75 µm respectively. Final gap size after pull-in (g_f) was 1 µm. Support springs were 2 µm (w_s) by 241 µm (l_s). Young's Modulus (E) and the relative permittivity of deionized water (ϵ_r) were estimated at 169 GPa and 80 respectively.

Each device was tested in deionized water using a 1 MHz AC square wave with zero-to-peak amplitudes from 0 V to 6 V. When this signal is first applied to the shuttle and moveable fingers, capacitive coupling through the water results in an attenuated 1 MHz signal at the sense-stop. When pull-in occurs, electrical contact is made between the shuttle and sense-stop and the full AC square wave is observed. This measurement procedure is outlined in Figure 3.

GCA pull-in time was measured for all finger lengths and varied in rough agreement with theoretical calculations (Figure 4). For long overlap lengths ($L \geq 70$ µm), experimental measurements demonstrated good agreement with the theory. For shorter overlap lengths ($L \leq 55$ µm), pull-in measurements were generally faster than predicted by theory. As overlap length decreases, observed divergence increases, suggesting that the dynamics model loses accuracy for small finger dimensions. Further analysis is required for a more complete model across finger dimensions.

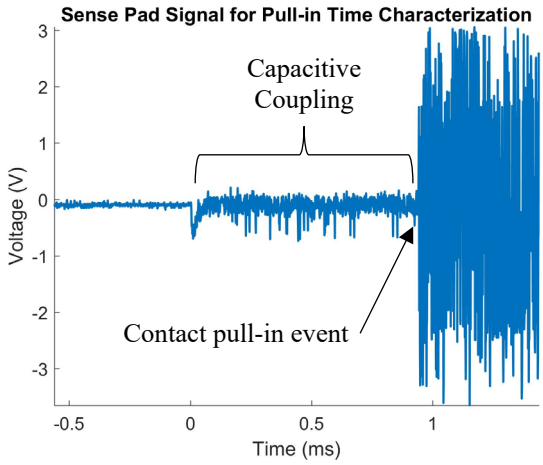

Figure 3: Capacitive coupling through water is observed starting at 0 ms and complete pull-in occurs at 0.94 ms.

Pull-in times across all devices were measured at less than 25 ms. The fastest pull-in time recorded was 121 µs for an overlap length of 10 µm and drive signal amplitude

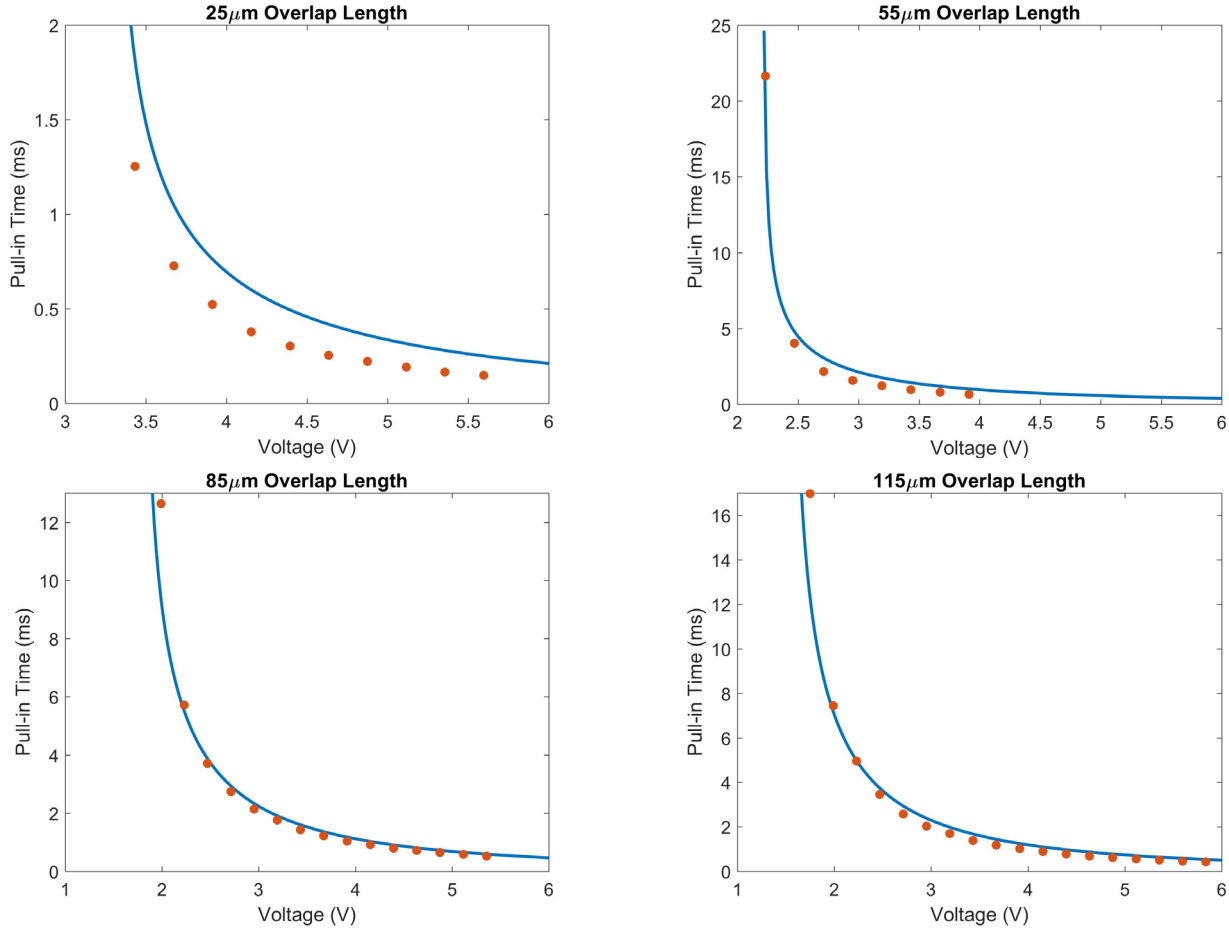

Figure 4: Pull-in time measurements (points) compared with theory (curves) across drive signal amplitudes for overlap lengths of L = 25 µm, 55 µm, 85 µm, and 115 µm. The 55 µm device was damaged before testing up to 6 V.

of 5 V, and the slowest pull-in time recorded was 23 ms for an overlap length of 130 µm and drive signal amplitude of 2.09 V. Compared to operation in air, GCAs with similar dimensions submerged in deionized water have slower pull-in times [8]. However, this reduction in actuation speed is offset by the substantial gain in force as a result of the relative permittivity factor. This factor was calculated to be within 18% of the estimated value of 80 on average based on the data in Figure 5, which demonstrates that aqueous environments confer a substantial increase in actuation force (refer to Equation 2). A GCA with L = 130 µm operating in liquid with $\epsilon_r = 80$ at 6 V drive signal amplitude could provide up to 4.6 mN of force with rapid actuation time, and an electrostatic inchworm motor using these GCAs would demonstrate large displacement, high force density, and fast actuation.

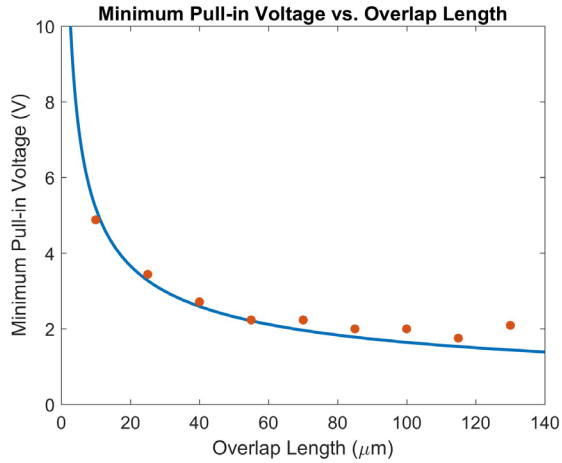

Figure 5: The minimum pull-in voltage required for a given overlap length in theory (curve) and experiment (points).

Preliminary tests on inchworm motors fabricated under the process described in [8] were performed and exhibited partial success with two of four GCAs actuating as expected (the remaining two experienced metal adhesion problems). With a Cr/Ru sputter, we expect to achieve full operation of submerged electrostatic inchworm motors. Additional preliminary tests were performed on GCAs in ionic solution. These devices were successfully tested in solutions of sodium dodecyl sulfate (SDS) up to concentrations of 10 mM. SDS also served as a surfactant, reducing bubble formation in etch holes and small features.

CONCLUSIONS

To date, operation of electrostatic MEMS actuators in aqueous conditions has been limited to moderate displacements and forces, and there has been little characterization of actuation speed. We demonstrate that gap-closing actuator arrays can operate at high speeds with low supply voltages. Based on our analysis of the relative permittivity factor, they can also produce actuation forces much larger than identical devices in air can produce. A submerged electrostatic inchworm motor based off of these devices should thus produce high force while achieving large displacements and fast shuttle speeds. We have observed partial success in driving an inchworm motor in deionized water and have successfully driven GCAs in ionic media (10 mM). These results are indications that inchworm motors driven by GCAs can operate in ionic media without encapsulation, which would enable many aqueous MEMS applications.

ACKNOWLEDGEMENTS

GCA devices were fabricated at the UC Berkeley Marvell Nanofabrication Laboratory. Many thanks to the Berkeley SWARM Lab residents for their encouragement and advice, and to the Summer Undergraduate Research Fellowship (SURF) program for its support and funding. Special thanks to Dr. Michel Maharbiz for his technical input, guidance, and inspiration.

REFERENCES

[1] D. Sameoto, T. Hubbard, M. Kujath, "Operation of Electrothermal and Electrostatic MUMPS Microactuators Underwater", *J. Micromech. Microeng.*, vol. 14, pp. 1359-1366, 2004.

[2] T. Sounart, T. Michalske, K. Zavadil, "Frequency-Dependent Electrostatic Actuation in Microfluidic MEMS", *J. Microelectromech. Syst.*, vol. 14, pp. 125-133, 2005.

[3] V. Mukundan, B. Pruitt, "MEMS Electrostatic Actuation in Conducting Biological Media", *J. Microelectromech. Syst.*, vol. 18, pp. 405-413, 2009.

[4] M. Erismis, H. Neves, P. Moor, R. Puers, C. Hoof, "A Water-Tight Packaging of MEMS Electrostatic Actuators for Biomedical Applications", *Microsyst. Technol.*, vol. 16, pp. 2109-2113, 2010.

[5] H. Panchawagh, T. Sounart, A. Kausik, D. Finch, R. Mahajan, "Characterization of Silicon Parallel-Plate Electrostatic Actuator in Partially Conducting Aqueous Solution", *Digest Tech. MEMS '08 Conference*, Wuhan, January 13-17, 2008, pp. 495-498.

[6] B. Preetham, M. Lake, D. Hoelzle, "A Curved Electrode Electrostatic Actuator Designed for Large Displacement and Force in an Underwater Environment", *J. Micromech. Microeng.*, vol. 27, pp. 1-8, 2017.

[7] I. Penskiy, S. Bergbreiter, "Optimized Electrostatic Inchworm Motors using a Flexible Driving Arm", *J. Micromech. Microeng.*, vol. 23, pp. 1-12, 2013.

[8] D. Contreras, K. Pister, "Dynamics of Electrostatic Inchworm Motors for Silicon Microrobots", in *Digest Tech. Papers MARSS '17 Conference*, Montréal, July 17-21, 2017, pp. 1-6.

[9] M. Bao, H. Yang, "Squeeze Film Air Damping in MEMS", *Sensors and Actuators A.*, vol. 136, pp. 3-27, 2007.

[10] M. Li, V. Rouf, D. Horsley, "Substrate Effect in Squeeze Film Damping of Lateral Oscillating Microstructures", *Digest Tech. MEMS '13 Conference*, Taipei, January 20-24, 2013, pp. 393-396.

[11] H. Over, "Surface Chemistry of Ruthenium Dioxide in Heterogeneous Catalysis and Electrocatalysis: From Fundamental to Applied Research", *Chem. Rev.*, vol. 112, pp. 3356-3426, 2012.

CONTACT

*R.M. Shih, tel: +1-904-881-4744; rmshih@berkeley.edu